PNAS RESEARCH ARTICLE | BIOCHEMISTRY

NgR1 binding to reovirus reveals an unusual bivalent interaction and a new viral attachment protein

Danica M. Sutherland[a,b], Michael Strebl[c], Melanie Koehler[d], Olivia L. Welsh[a,b], Xinzhe Yu[e], Liya Hu[e], Rita dos Santos Natividade[d], Jonathan J. Knowlton[a,f], Gwen M. Taylor[a,b], Rodolfo A. Moreno[e], Patrick Wörz[c], Zachery R. Lonergan[f], Pavithra Aravamudhan[a,b], Camila Guzman-Cardozo[a,b], Sukhleen Kour[a], Udai Bhan Pandey[a,g,h], David Alsteens[d,i], Zhao Wang[e,j,k], B. V. Venkataram Prasad[e,l], Thilo Stehle[c], and Terence S. Dermody[a,b,m,1]

Edited by Harmit Malik, Fred Hutchinson Cancer Center, Seattle, WA; received November 14, 2022; accepted April 19, 2023

Nogo-66 receptor 1 (NgR1) binds a variety of structurally dissimilar ligands in the adult central nervous system to inhibit axon extension. Disruption of ligand binding to NgR1 and subsequent signaling can improve neuron outgrowth, making NgR1 an important therapeutic target for diverse neurological conditions such as spinal crush injuries and Alzheimer's disease. Human NgR1 serves as a receptor for mammalian orthoreovirus (reovirus), but the mechanism of virus–receptor engagement is unknown. To elucidate how NgR1 mediates cell binding and entry of reovirus, we defined the affinity of interaction between virus and receptor, determined the structure of the virus–receptor complex, and identified residues in the receptor required for virus binding and infection. These studies revealed that central NgR1 surfaces form a bridge between two copies of viral capsid protein σ3, establishing that σ3 serves as a receptor ligand for reovirus. This unusual binding interface produces high-avidity interactions between virus and receptor to prime early entry steps. These studies refine models of reovirus cell-attachment and highlight the evolution of viruses to engage multiple receptors using distinct capsid components.

Nogo receptor 1 | receptor | structure | virus | attachment

Significance

Neuronal plasticity is an essential process in central nervous system (CNS) development and is coordinated in part by a key scaffold protein called NgR1. NgR1 also functions as a receptor for reovirus, a CNS-tropic virus capable of causing encephalitis in young mammals. Despite the important role of NgR1 in brain homeostasis, structural information guiding an understanding of NgR1 interactions with its ligands is lacking. Here, we describe in molecular detail how NgR1 uses its predicted key scaffolding surface to bind reovirus, which revealed a noncanonical viral ligand for this pathogen. These studies highlight how viruses employ multiple capsid components to engage host receptors and often target receptor surfaces required for interaction with host proteins with essential, conserved functions.

Every virus must cross host membranes to deliver its genetic payload to the interior of the cell. To overcome this membrane barrier, viruses must engage host receptors expressed on the cell surface or in endosomal compartments to mediate adhesion, internalization, and disassembly. For many viruses, accessing the cytoplasm requires more than just a single viral capsid component binding to a single host receptor. Instead, virus–receptor interactions often require many components of the viral capsid to engage different host molecules over space and time to orchestrate this critical step in infection. This coordinated first encounter between virus and host influences all subsequent events, including disease type and severity.

Mammalian orthoreovirus (reovirus) provides a highly tractable and well-established experimental system to study mechanisms of viral receptor engagement and how receptor use influences disease. Reovirus virions are nonenveloped, double-shelled particles that undergo stepwise binding to host cells and proteolytic disassembly prior to releasing transcriptionally active viral cores into the cytosol (1). Reovirus causes age-restricted disease in many mammalian species (2–4) and readily infects humans (5–8). In mice, reovirus disseminates from initial sites of replication in either the intestine or lung to produce strain-specific patterns of tropism in the brain and concomitant disease (9, 10). Serotype 1 (T1) reovirus strains infect ependymal cells lining the ventricles of the brain and cause a nonlethal hydrocephalus (9), whereas serotype 3 (T3) strains infect neurons in the central nervous system (CNS) and produce a fulminant, and often lethal, encephalitis (10). These differences in tropism and disease are mediated by the σ1 viral attachment protein and are thought to be dictated by differences in receptor use (10, 11).

Most reovirus strains use a multistep binding process, engaging sequential cell-surface receptors with i) low affinity, ii) high affinity, and iii) internalization functions to drive uptake of reovirus virions, disassembly to form infectious subvirion particles (ISVPs) (Fig. 1*A*), and penetration into the cytosol. Two reovirus outer-capsid proteins mediate these binding events—the σ1 viral attachment protein and the λ2 base into which σ1 inserts. Different domains of T1 and T3 σ1 proteins bind to different sialylated carbohydrates with low affinity (12, 13), suggesting independent evolution of this binding activity for reovirus. Glycan engagement promotes adhesion strengthening of reovirus to the cell surface (14) and enhances affinity of the virus for other receptors, possibly by promoting conformational changes in the viral particle (15). Requirements for virus binding to sialic

Author contributions: D.M.S., M.S., M.K., S.K., U.B.P., D.A., B.V.V.P., T.S., and T.S.D. designed research; D.M.S., M.S., M.K., O.L.W., X.Y., L.H., R.d.S.N., J.J.K., G.M.T., R.A.M., P.W., Z.R.L., and S.K. performed research; D.M.S., P.A., C.G.-C., S.K., U.B.P., and Z.W. contributed new reagents/analytic tools; D.M.S., M.S., M.K., O.L.W., R.d.S.N., and J.J.K. analyzed data; and D.M.S., M.S., M.K., S.K., U.B.P., D.A., B.V.V.P., T.S., and T.S.D. wrote the paper.

The authors declare no competing interest.

This article is a PNAS Direct Submission.

Copyright © 2023 the Author(s). Published by PNAS. This article is distributed under Creative Commons Attribution-NonCommercial-NoDerivatives License 4.0 (CC BY-NC-ND).

[1]To whom correspondence may be addressed. Email: terence.dermody@chp.edu.

This article contains supporting information online at https://www.pnas.org/lookup/suppl/doi:10.1073/pnas.2219404120/-/DCSupplemental.

Published June 6, 2023.

Downloaded from https://www.pnas.org by UNIVERSITE CATHOLIQUE DE LOUVAIN (UCL) SERVICE CENTRAL DES BIBLIOTHEQUES on January 16, 2024 from IP address 130.104.43.178.

acid differ by cell type and virus strain (12, 13, 16), and efficient glycan engagement influences viral virulence (17–19).

The σ1 protein also binds junctional adhesion molecule-A (JAM-A), an immunoglobulin (Ig) superfamily protein, using a mechanism conserved between the viral serotypes (20, 21). JAM-A expression on endothelial cells promotes reovirus viremia and hematogenous dissemination in the host (22, 23). However, despite the high affinity of reovirus σ1 for JAM-A, this receptor does not initiate signaling required for endosomal internalization (24). Instead, conserved sequence motifs in the viral λ2 protein promote binding to integrins, clathrin recruitment, and efficient cell entry (24, 25). Binding to either sialic acid or JAM-A is dispensable for reovirus replication in the intestine and brain. Thus, there are key gaps in knowledge about reovirus receptor use and function in different tissues.

Human Nogo-66 receptor 1 (NgR1) was identified as a reovirus receptor in an RNA interference screen (26). In contrast to JAM-A, which can bind both virions and ISVPs, NgR1 selectively binds virions (26). ISVPs are characterized by an altered conformer of the σ1 protein and proteolytic removal of the σ3 protein, leading to the hypothesis that the virion conformer of σ1, outer-capsid protein σ3, or both engage NgR1. NgR1 is expressed in neural cells targeted by reovirus (23, 27–29) and interacts with a structurally diverse set of myelin inhibitory proteins to recruit multiple coreceptors, initiate signaling, and prevent neurite outgrowth (30–33). There is limited structural information about how NgR1 coordinates binding to these diverse ligands and coreceptors to mediate its functions. However, disruption of NgR1 interactions with these ligands can promote nerve growth recovery (34–37). Thus, an enhanced understanding of the structural basis of NgR1–ligand interactions may foster development of therapeutics.

In this study, we used a combination of biophysical, biochemical, and genetic strategies to define interactions between reovirus and NgR1. We identified that the viral outer-capsid protein σ3 engages NgR1, establishing an additional viral ligand for reovirus. Two neighboring σ3 proteins ligate conserved sequences of a single NgR1 molecule, a mechanism that likely promotes the high avidity of interactions observed between virus and receptor and catalyzes early infection steps. Collectively, these studies enhance an

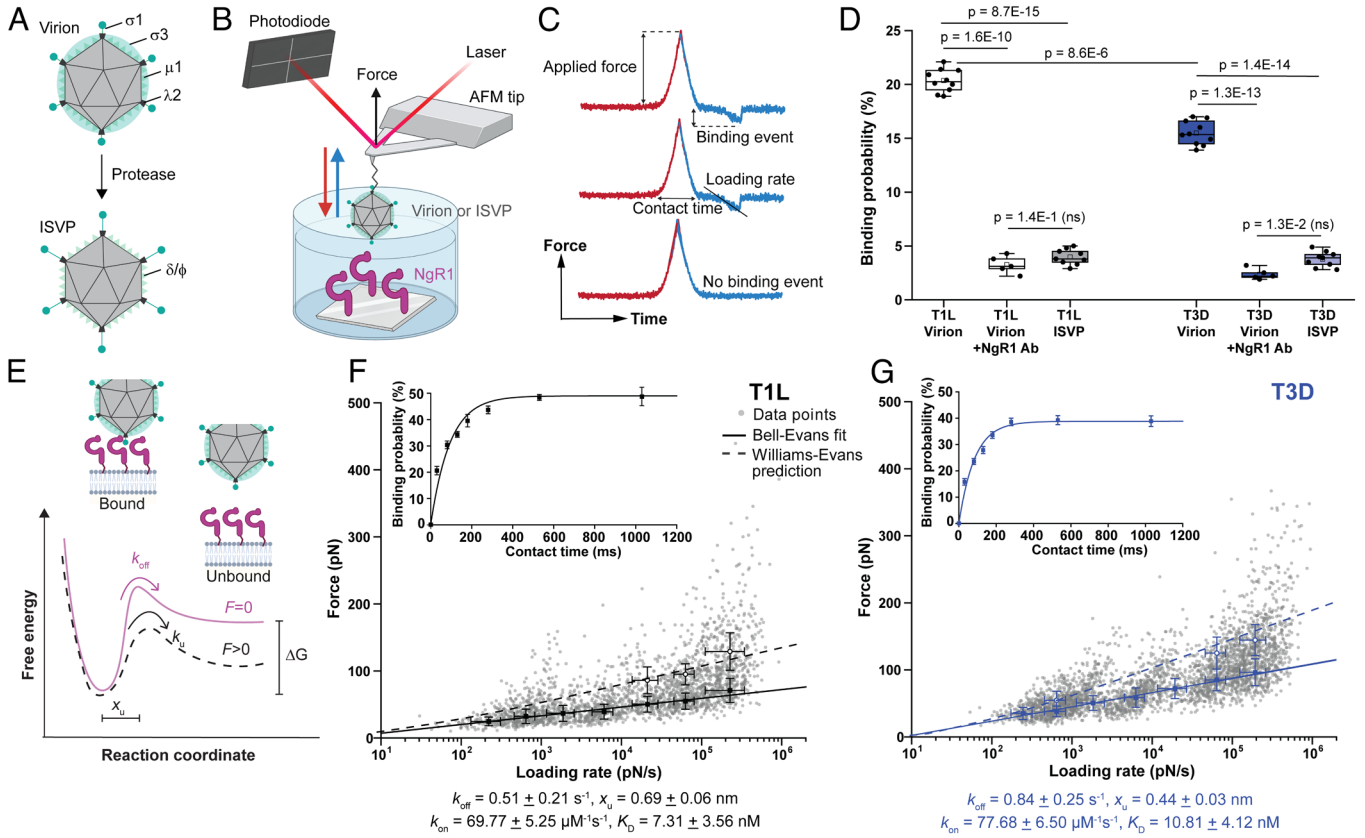

Fig. 1. Reovirus virions bind to NgR1 on model surfaces with high affinity. (*A*) Schematic of reovirus virions and ISVPs showing loss of outer-capsid protein σ3, cleavage of μ1 to δ and φ fragments, and extension of the σ1 protein in ISVPs. (*B*) Schematic of probing reovirus particle binding to NgR1 using AFM. Pixel-for-pixel, force-distance, curve-based AFM is used to approach and retract the sample from a tip attached to a cantilever and record interaction forces, *F*, over the tip-sample distance in force-distance curves. Made using BioRender. (*C*) Force-time curve from which the loading rate can be extracted from the slope of the curve immediately before bond rupture (loading rate = $\Delta F/\Delta t$) (upper curve). The contact time is the interval in which the tip and surface are in constant contact (middle curve). The lower curve shows no binding events. Made using BioRender. (*D*) Box plot summarizing the binding probability from AFM studies for the conditions shown. Each data point represents the binding probability from one map acquired at a retraction speed of 1 μm/s. Mean (*Inset* square), median (horizontal line), 25th and 75th percentiles, and highest and lowest values (whiskers) are shown. N = 10 maps examined for three independent experiments. *P* values were determined by the two-sample *t* test. (*E*) Bell–Evans model describing a virus–receptor interaction as a two-state model (BioRender). The bound state is separated from the unbound state by a single energy barrier located at distance x_u. k_{off} and k_{on} represent the dissociation and association rates, respectively. (*F* and *G*) DFS plot showing the distribution of average rupture forces, determined at seven distinct loading-rate (LR) ranges, quantified between NgR1 and either T1L (*F*) or T3D (*G*) virions. Data corresponding to single interactions were fit with the Bell–Evans model (solid black or blue line, respectively), providing average k_{off} and x_u values. Dashed lines represent predicted binding forces for multiple simultaneous uncorrelated interactions ruptured in parallel (Williams–Evans prediction). Inserted graphs: Binding probability is plotted as a function of the contact time. Least-squares fits of the data to a monoexponential decay curve (line) provides average kinetic on-rates (k_{on}) of the probed interaction. Further calculation (k_{off}/k_{on}) determines the KD. Each data point represents the binding force from one map acquired at a retraction speed of 1 μm/s for the different hold times. All experiments were conducted at least three times with independent tips and samples. Error bars indicate SD of mean values.

Downloaded from https://www.pnas.org by UNIVERSITE CATHOLIQUE DE LOUVAIN (UCL) SERVICE CENTRAL DES BIBLIOTHEQUES on January 16, 2024 from IP address 130.104.43.178.

understanding of reovirus binding and entry events and provide an in-depth visualization of an NgR1–ligand interface.

Results

Reovirus Binds NgR1 on Receptor-Coated Surfaces with High Avidity. To determine the affinity of virus binding to NgR1 and clarify whether there are strain-specific differences in the capacity of reovirus to bind NgR1, we used force-distance-based atomic force microscopy. This approach allows real-time observations of rare and transient binding events and precise quantification of single-molecule interactions. Virions or ISVPs of prototype T1 and T3 reovirus strains, T1L and T3D, were covalently linked to an atomic force microscopy (AFM) probe tip, and interactions with a surface coated with purified, full-length NgR1 protein were kinetically and thermodynamically probed (Fig. 1*B*). The AFM tip was cyclically contacted and retracted from the NgR1-coated surface, and the force between the viral-particle-functionalized tip and the surface was monitored over time (Fig. 1*C*; force vs. time curves). Virions of both strains displayed high binding probability to the NgR1-coated surface (Fig. 1*D*). Importantly, preincubation of model surfaces with an NgR1-specific antibody abolished binding by virions and, consistent with previous studies (26), ISVPs were incapable of NgR1 engagement (Fig. 1*D*).

As T1L virions were ~30% more likely to bind the NgR1-coated surface than were T3D virions (Fig. 1*D*), we speculated that sequence polymorphisms in the viral ligand might be responsible for this difference. Between these strains, the σ3 proteins share ~97% identity, and the σ1 proteins share ~27% identity (38). To determine whether the T1L σ1 sequences mediate more efficient NgR1 engagement, we assessed the binding of reovirus strain T3SA+, which is structurally identical to T1L apart from a T3D-like σ1 protein. T3SA+ virions bound NgR1 comparably to T1L virions (*SI Appendix*, Fig. S1*A*), suggesting that the σ1 viral attachment protein does not mediate reovirus binding to NgR1.

We next defined the kinetic properties of reovirus–NgR1 bonds by probing the interaction at various loading rates (e.g., force applied over time) (39). Fitting the data with the Bell-Evans model (Fig. 1*E*) (40, 41) enabled us to extract the dissociation rate (k_{off}) and the distance to the transition state (x_u) for T1L (Fig. 1*F*) and T3D (Fig. 1*G*). Overall, there was a slightly higher distance to the transition state for T1L virions relative to T3D virions, indicating an increase in conformational variability following binding to NgR1 as well as a diminished dissociation rate, suggesting more stable interactions. Higher forces on dynamic force spectroscopy (DFS) plots originate from the failure of uncorrelated bonds in parallel, as predicted by the Williams–Evans model (42). We observed a high correlation between the William–Evans predictions and recorded single-molecule data. These findings suggest that reovirus virions establish multivalent interactions with NgR1.

By monitoring the influence of contact time on binding probability (Fig. 1 *F* and *G*; *Insets*), we estimated the association rate (k_{on}) by assuming that the receptor-bound complex can be approximated by pseudo-first-order kinetics (43) and calculated equilibrium dissociation constants (K_D) for the studied complexes (k_{off}/k_{on}). All three strains tested demonstrated K_D values in the nM range (~7 to 11 nM), indicating high-affinity interactions and further confirming the stability of the complexes established by reovirus and NgR1 (*Insets*, Fig. 1 *F* and *G* and *SI Appendix*, Fig. S1 *B* and *C*). Similar values have been reported for other reovirus–receptor interactions (14, 25, 44). However, the slightly higher binding probability of T1L and T3SA+ for NgR1 relative to T3D provides further evidence that sequence polymorphisms displayed by the σ1 protein do not explain differences in biophysical interaction parameters with NgR1.

Reovirus Virions Bind to NgR1 on Living Cells. To determine whether interactions probed on isolated NgR1 receptors are established in the context of living cells, we used Chinese hamster ovary (CHO) Lec2 cells engineered to express NgR1. CHO Lec2 cells do not efficiently express cell-surface sialic acid (45) and bind reovirus poorly (15) due to the absence of reovirus receptors. Using AFM tips functionalized with either T1L or T3D virions, we probed monolayers of cocultured Lec2 cells, fluorescently labeled with a nuclear protein H2B-eGFP and actin-mCherry, and unlabeled NgR1-expressing Lec2 cells (Lec2-NgR1) (Fig. 2*A*). Fields of view were chosen in which both cell types were adjacent, serving as direct internal controls. AFM height images (Fig. 2 *B* and *C*; *Upper*) were recorded together with corresponding adhesion images, revealing the location of specific adhesion events displayed as bright pixels (Fig. 2 *B* and *C*; *Lower*). Lec2-NgR1 cells demonstrated a high density of adhesion events, ~ 9% for T1L and ~ 6% for T3D (Fig. 2*D*), whereas Lec2 cells displayed only a sparse distribution of these events, < 2% (Fig. 2*D*), suggesting NgR1-specific attachment of reovirus to living cells. Specificity of the probed interactions was validated by treatment with an NgR1-specific antibody prior to adsorption, which led to a significant decrease in binding to Lec2-NgR1 cells. Similar to our findings using model surfaces, we observed a modest increase in binding to Lec2-NgR1 cells by T1L and T3SA+ relative to T3D (*SI Appendix*, Fig. S1 *D–G*). Specific binding forces and corresponding loading rates were extracted from force vs. time curves recorded on Lec2-NgR1 cells and overlaid on the DFS plots obtained using NgR1-coated surfaces (Fig. 2 *E* and *F* and *SI Appendix*, Fig. S1*G*). Data obtained using purified receptors and living cells aligned well, confirming the relevance of results obtained using model surfaces. Collectively, these data demonstrate that multiple reovirus strains bind NgR1 with high affinity.

NgR1 Homologs Do Not Support Reovirus Infection. NgR1 displays a canonical leucine-rich-repeat (LRR) protein fold (46, 47) (Fig. 3*A*) that also is observed in pathogen-sensing proteins (48–50). Eight tandem LRRs of NgR1 are appended on either end with noncanonical leucine-rich (LR) domains, and the C terminus of the protein is capped by a large domain of unknown structure that anchors NgR1 to the cell membrane by a glycophosphatidylinositol (GPI) moiety (Fig. 3*A*). NgR1 has two homologs, NgR2 and NgR3, that display partial functional redundancy with NgR1 (51–53). To test whether NgR2 and NgR3 also serve as reovirus receptors, we transfected CHO cells with plasmids encoding NgR1, NgR2, or NgR3. Expression of NgR1 and NgR2 (for which there are commercially available antibodies) (Fig. 3*B*), reovirus binding, and infection of transfected cells were assessed. Mock transfection or expression of coxsackie virus and adenovirus receptor (CAR) were used as negative controls. NgR1, but not NgR2 or NgR3, promoted reovirus binding (Fig. 3*C*) and infection (Fig. 3*D*), indicating that NgR1 serves as a specific receptor for reovirus. Since NgR3 expression could not be confirmed, these data do not exclude the possibility that NgR3 serves as a reovirus receptor.

NgR1 Engages the σ3 Outer-Capsid Protein. NgR1 promotes binding and infection of reovirus virions but not ISVPs (26). This particle-specific binding capacity suggests that the more compact virion conformer of σ1, outer-capsid protein σ3, or some combination of these capsid components functions as the viral

Downloaded from https://www.pnas.org by UNIVERSITE CATHOLIQUE DE LOUVAIN (UCL) SERVICE CENTRAL DES BIBLIOTHEQUES on January 16, 2024 from IP address 130.104.43.178.

Downloaded from https://www.pnas.org by UNIVERSITE CATHOLIQUE DE LOUVAIN (UCL) SERVICE CENTRAL DES BIBLIOTHEQUES on January 16, 2024 from IP address 130.104.43.178.

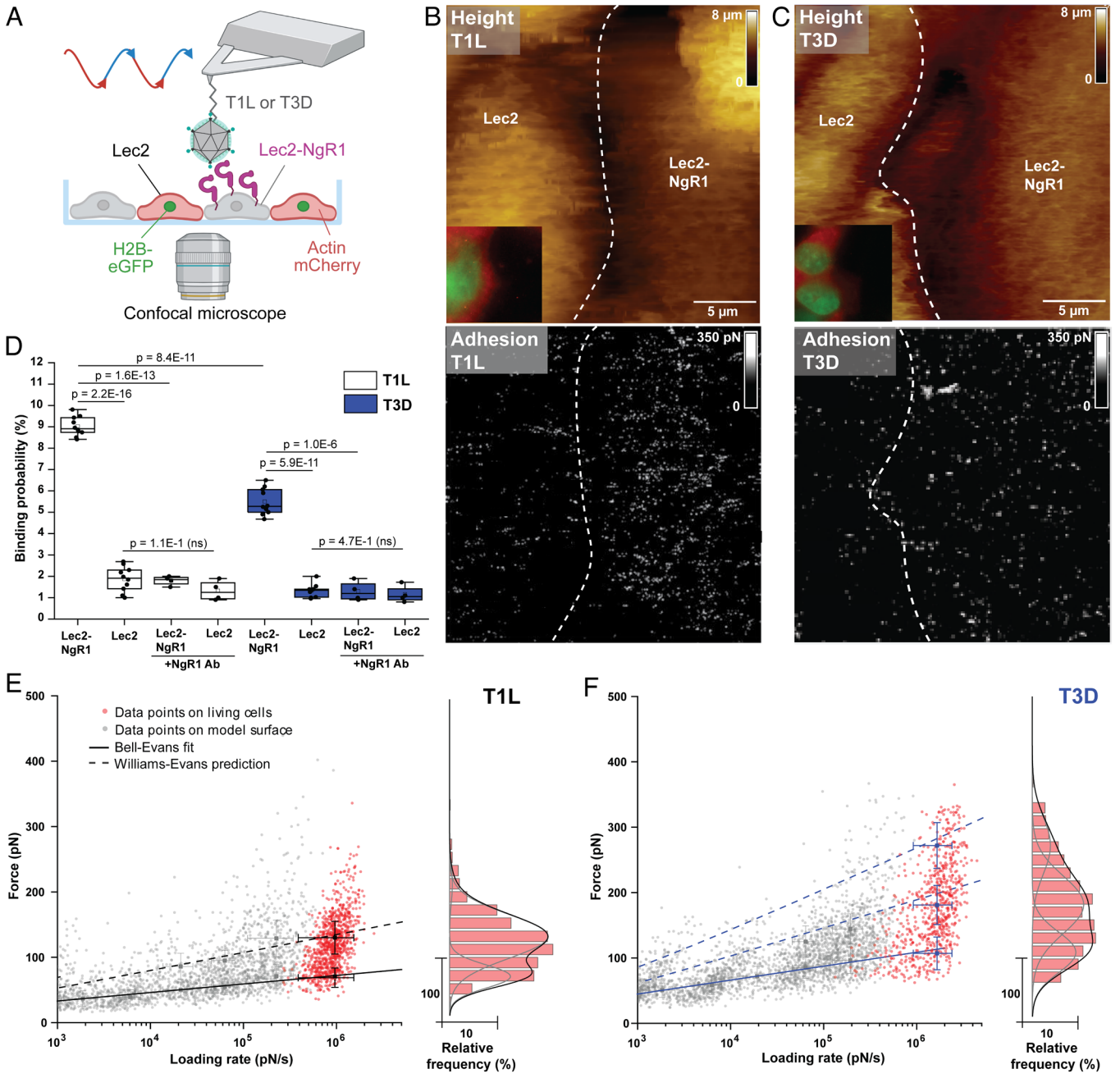

Fig. 2. Reovirus virion binding to NgR1 on living cells mirrors binding to NgR1 on model surfaces. (*A*) Schematic (BioRender) depicting reovirus virions probed on a confluent layer of cocultured fluorescent Lec2 (actin-mCherry and H2B-eGFP) and Lec2-NgR1 cells by combined optical microscopy and force-distance-based AFM. (*B* and *C*) Corresponding representative images of force-distance-based AFM topography (*Top*), confocal microscopy (*Top*, *Inset*), and adhesion map (*Bottom*) from probing adjacent Lec2 and Lec2-NgR1 cells with either T1L (*B*) or T3D (*C*) virions coupled to the AFM tip. Adhesion maps show interactions (white pixels) primarily with Lec2-NgR1 cells. (*D*) Box plot of the binding probability between either T1L (white) or T3D (blue) virions and Lec2 or Lec2-NgR1 cells, before and after injection of NgR1-specific antibody (Ab). Box-and-whisker plot is displayed as described above. For experiments without injection of NgR1-specific antibody, the data were obtained from at least N = 10 cells from four independent experiments. Data for blocking experiments were obtained from at least N = 4 cells from two independent experiments. *P*-values were determined by the two-sample *t* test. (*E* and *F*) DFS plots showing the distribution of rupture forces quantified between either T1L (*E*) or T3D (*F*) virions and NgR1-expressing Lec2 cells (red data points). Data points in gray represent rupture forces quantified using NgR1 model surfaces (extracted from Fig. 1 *F* and *G*, respectively). Histograms of the force distribution observed on cells fitted with a multi-peak Gaussian distribution (N > 800 data points) are shown at the sides. Error bars indicate SD of the mean values.

ligand for NgR1. To identify the viral NgR1 ligand, we evaluated whether soluble, recombinant NgR1 can interact with isolated σ1 protein or σ3 protein. The virion particle contains a σ1 trimer at each of the 12 icosahedral vertices as well as 200 heterohexamers of σ3 and µ1 ($\sigma3_3\mu1_3$) (Fig. 4*A*). Recombinant σ1 and $\sigma3_3\mu1_3$ (Fig. 4*B*) were purified and incubated with NgR1-Fc as an affinity ligand in a bead-based binding assay. Surprisingly, NgR1 bound to $\sigma3_3\mu1_3$ complexes (Fig. 4 *C* and *D*) but not to the classically defined viral attachment protein, σ1 (*SI Appendix*, Fig. S2). This binding is specific, as the unrelated CAR protein was unable to precipitate $\sigma3_3\mu1_3$.

To determine whether σ3 alone is capable of binding NgR1, we incubated radiolabeled σ3 with CAR-Fc, NgR1-Fc, or a σ3-specific antibody, and Fc-expressing proteins were precipitated and analyzed for bound radiolabeled σ3. When expressed without µ1, σ3 forms dimers (Fig. 4*A*) (55), shielding some surfaces that would otherwise be exposed in the virion-associated conformer of σ3. Remarkably, isolated σ3 bound NgR1 effectively (Fig. 4 *E* and *F*). Collectively,

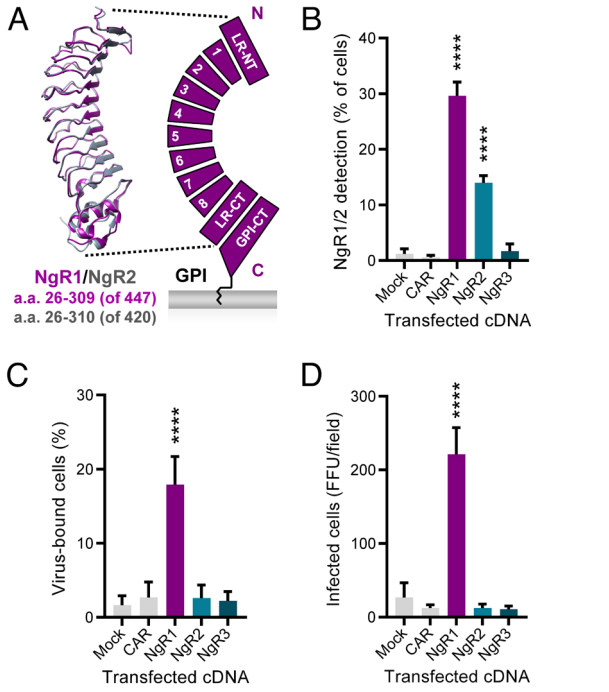

Fig. 3. NgR1 is a specific receptor for reovirus. (*A*) Ribbon tracings of partial NgR1 (purple) (46) and NgR2 (gray) (54) ectodomains alongside a schematic of NgR1 [leucine-rich (LR) repeat (LRR) 1-8; GPI]. N and C termini are indicated. Schematic not to scale. (*B–D*) CHO cells were mock-transfected or transfected with the cDNAs shown and incubated for 48 h. (*B*) NgR1 and NgR2 expression was detected on the cell surface by flow cytometry using pooled NgR1 and NgR2 antibodies. (*C*) Transfected cells were incubated on ice with reovirus strain T3SA− for 1 h. Reovirus binding was detected by flow cytometry using reovirus-specific antiserum. (*D*) Transfected cells were incubated with T3SA− at room temperature for 1 h. At 24 hpi, infectivity was quantified by FFU assay. Error bars indicate SD. Values that differ significantly from mock by one-way ANOVA and Dunnett's test are indicated (****$P < 0.0001$).

these data reveal that the reovirus σ3 outer-capsid protein is a viral ligand for cell receptors and expand known reovirus ligands to now include three capsid components (σ1, λ2, and σ3).

Cryo-Electron Microscopy (Cryo-EM) Reconstructions Reveal that NgR1 Bridges Two σ3 Outer-Capsid Proteins. To elucidate the structure of NgR1 bound to σ3, we conducted cryo-EM analyses of NgR1 bound to whole virions. Purified virions were incubated alone (Fig. 5*A*) or with NgR1 a.a. 26-310 (Fig. 5*B*), a stable ectodomain fragment we confirmed is responsible for reovirus engagement (*SI Appendix*, Fig. S3). Samples were visualized using cryo-EM, and images of virions alone (5,954 particles) or virions in complex with NgR1 (1,648 particles) were used to determine three-dimensional (3D) reconstructions at final resolutions of 7.2 Å and 8.9 Å, respectively (*SI Appendix*, Fig. S4). Icosahedral symmetry of the virion, which was applied during reconstructions based on the known structure of reovirus virions (56, 57), is highlighted at the twofold, threefold, and fivefold axes of symmetry in both reconstructions (Fig. 5 *C–F*). Importantly, additional density was observed at the surface of virions complexed with NgR1, which is apparent in cross-sections of the reconstructions (Fig. 5*D*, arrowheads) and in a 3D overview in which additional density appears in a star-like pattern overlying σ3 proteins (Fig. 5*F* and Movie S1). Consistent with coprecipitation assays (Fig. 4 *E* and *F*), these data conclusively demonstrate that NgR1 binds to σ3.

To obtain molecular detail of the σ3–NgR1 binding interface, we placed available protein structures into the cryo-EM reconstructions. Only the asymmetric unit of the virion, which can be tiled 60 times to build a particle in silica, is shown for simplicity (Fig. 5 *G–I*). Each asymmetric unit consists of one copy each of λ2, σ2, and λ1, and 10 copies each of μ1 and σ3. These 10 protomers of μ1 and σ3 compose three full heterohexamers (Fig. 5*H*, indicated by black triangles) and one third of a fourth heterohexamer, which is located at a threefold symmetry axis. The flexibility, trimeric nature, and incomplete occupancy of the σ1 fiber prevents full resolution of this protein in particle-averaged reconstructions, but remnants of the fiber base embedded into the λ2 pentamer are occasionally detected (Fig. 5*E*, blue nub above yellow) (57). Within the asymmetric unit of the reovirus–NgR1 reconstructions, five NgR1 molecules fit well within the remaining cryo-EM features

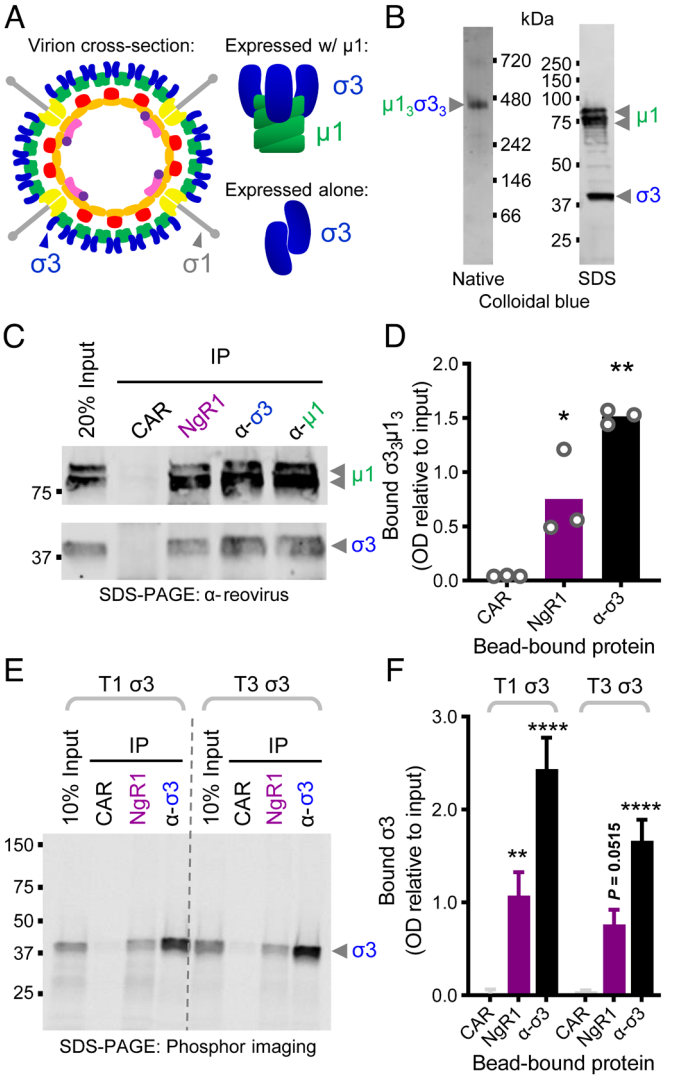

Fig. 4. Reovirus outer-capsid protein σ3 is the viral ligand for NgR1. (*A*) Schematic of reovirus capsid components. (*B*) Purified σ3$_3$μ1$_3$ analyzed using native polyacrylamide gel electrophoresis (PAGE) (*Left*) or sodium dodecyl sulfate (SDS)-PAGE (*Right*) and stained with colloidal blue. (*C* and *D*) Soluble Fc-tagged CAR or NgR1 or monoclonal antibodies 10C1 (σ3-specific) or 8H6 (μ1-specific) were immobilized onto protein G beads. Protein-conjugated beads were incubated with purified σ3$_3$μ1$_3$. Beads were washed and boiled, and released proteins were electrophoresed by SDS-PAGE and visualized using reovirus-specific antiserum. A representative gel (*C*) and quantification of three independent experiments (*D*) are shown. Values that differ significantly from CAR by one-way ANOVA and Dunnett's test are indicated (*$P < 0.05$; **$P < 0.01$). (*E* and *F*) Soluble Fc-tagged CAR or NgR1 or 10C1 (σ3-specific) monoclonal antibody were incubated with rabbit reticulocyte lysates expressing radiolabeled T1L or T3D σ3 and bound to beads. Beads were washed and boiled, and released proteins were subjected to SDS-PAGE. Immunoprecipitated proteins were visualized by phosphor imaging. A representative gel (*E*) and quantification of five independent experiments (*F*) are shown. SEM is shown. Values that differ significantly from CAR by two-way ANOVA and Tukey's test are indicated (**$P < 0.01$; ****$P < 0.0001$).

Downloaded from https://www.pnas.org by UNIVERSITE CATHOLIQUE DE LOUVAIN (UCL) SERVICE CENTRAL DES BIBLIOTHEQUES on January 16, 2024 from IP address 130.104.43.178.

Downloaded from https://www.pnas.org by UNIVERSITE CATHOLIQUE DE LOUVAIN (UCL) SERVICE CENTRAL DES BIBLIOTHEQUES on January 16, 2024 from IP address 130.104.43.178.

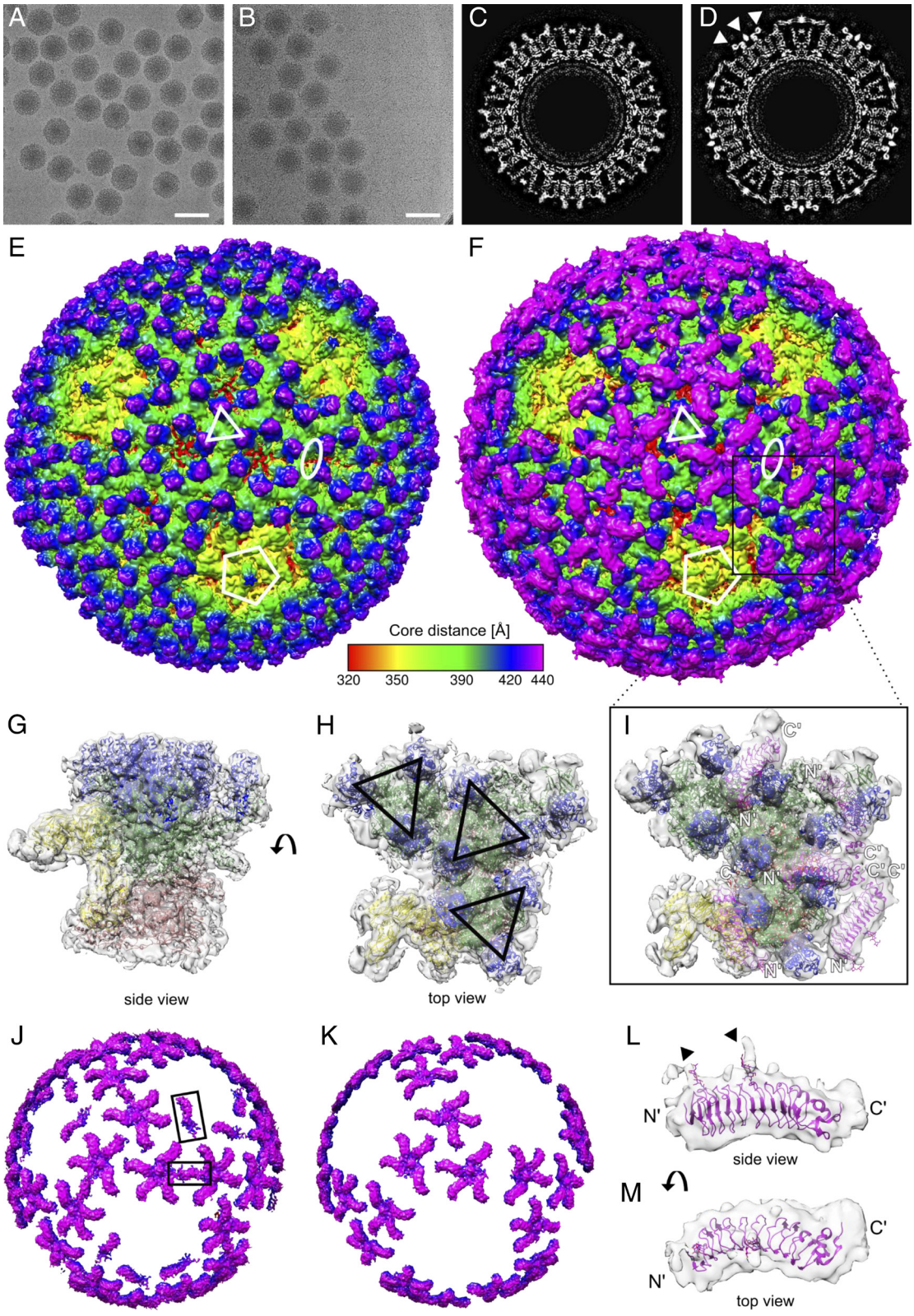

Fig. 5. Cryo-EM reconstruction of NgR1 bound to reovirus virions reveals a bivalent interaction mode. (*A* and *B*) Representative cryo-electron micrographs of reovirus virions alone (*A*) or complexed with NgR1 (*B*). Scale bar, 100 nm. (*C* and *D*) Central slices of the 3D cryo-EM reconstruction of reovirus virions alone (*C*) or complexed with NgR1 (*D*). White arrowheads indicate NgR1 density. (*E* and *F*) Overview of 3D reconstructions of reovirus virions alone (*E*) or complexed with NgR1 (*F*) at resolutions of 7.2 Å and 8.9 Å, respectively. Maps are colored by distance from the virus center (320 Å to 440 Å). Representative twofold, threefold, and fivefold symmetry axes of the icosahedral capsid are indicated by white symbols. (*G–I*) Asymmetric units for reovirus (*G*, side view; *H*, top view) or reovirus-NgR1 (*I*, top view). Ribbon tracings of reovirus proteins (σ3-blue, μ1-green, λ2-yellow, λ1-red, and σ2-red) and NgR1 (magenta) were placed into the 3D reconstructions (gray translucent surface representation) of virions (*G* and *H*) or the virion-NgR1 complex (*I*). (*H*) Individual $\sigma3_3\mu1_3$ heterohexamers are indicated with black triangles. (*I*) N and C termini for docked NgR1 molecules are labeled in white. (*J* and *K*) Difference density maps of the reovirus virion reconstruction subtracted from the reovirus-NgR1 reconstruction at sigma level 1.5 (*J*) or 2.0 (*K*). Major additional NgR1 features are indicated by black rectangles. (*L* and *M*) Side and top views of NgR1 ribbon tracing placed into the difference density map (sigma level = 1.15). Glycosylations are shown in stick format, and densities attributable to glycosylation are indicated by black arrowheads. N′ and C′ termini are indicated.

(Fig. 5*I*) and display binding modes comparable to each other (*SI Appendix*, Fig. S5). Four of these NgR1 molecules are embedded between two σ3 monomers of neighboring heterohexamers, while the fifth NgR1 molecule is located adjacent to the fivefold vertex and thus is flanked by only one σ3 monomer. This structure surprisingly reveals that two binding faces can be used by both NgR1 and σ3. Moreover, NgR1 density is distant from σ1 and μ1, confirming a specific interaction of the receptor with σ3.

To define additional features of the reovirus–NgR1 interaction, we subtracted the density of the reovirus virion reconstruction from that of the reovirus–NgR1 reconstruction and evaluated the resulting difference density map at various threshold levels (Fig. 5 *J* and *K*). NgR1 can be unambiguously placed in all five of the binding sites in the asymmetric unit (*SI Appendix*, Fig. S5). We also detected another feature in the difference density map located at the twofold symmetry axes of the virion surface (Fig. 5 *F* and *J*). This density is not shaped like a single NgR1 molecule but instead resembles an average of two NgR1 molecules, each bound in opposing directions. Therefore, accurate placement of the NgR1 coordinates into this density was not possible. However, the location of the density between σ3 monomers of adjacent hexamers is consistent with the NgR1-binding mode detected nearby on the particle. Increasing the threshold level of the difference density map from 1.5 to 2.0 removes this feature, along with the NgR1 moieties observed at the fivefold vertex (Fig. 5 *J* and *K*). This signal loss suggests weaker NgR1 density at these positions, which might be caused by decreased binding affinity at these sites.

The correct orientation of NgR1 is readily confirmed by the glycosylation signatures at N82 and N179, which are observed at a slightly lower threshold level (1.15) (Fig. 5 *L* and *M*). These glycan chains face away from the virion surface, which likely explains why they do not contribute to reovirus binding and infection (*SI Appendix*, Fig. S6). This orientation allows the His tag appended to NgR1, which replaces the GPI-CT of full-length NgR1, to accumulate at the center of four-to-five bound NgR1 molecules (Figs. 5*I* and 6*A*), suggesting a role for NgR1 oligomerization in binding to reovirus.

Residues on Two Faces of NgR1 Are Required for Efficient Reovirus Binding. By identifying NgR1 residues within 5 Å of σ3 (Fig. 6*B*), we predict two major interaction interfaces, a smaller surface on the convex face of NgR1 and a significantly larger one on the more-conserved concave face of NgR1 (Fig. 6*B*). The smaller surface consists mostly of glutamines and glutamates that could potentially form electrostatic or polar interactions (Fig. 6*C*). The larger surface is defined by a broad patch of aromatic residues within a central cavity emanating from NgR1 L208 (Fig. 6*D*). This binding surface provides possibilities for charged, polar, or hydrophobic interactions (*SI Appendix*, Fig. S7).

To define NgR1 residues required for binding to σ3, we used the reovirus–NgR1 structure to rationalize mutations at the small ($\sigma3_A$) and large ($\sigma3_B$) interaction interfaces. We hypothesized that disruption of NgR1 residues in close proximity to σ3 (< 5 Å) would abolish virus binding, whereas disruption of NgR1 residues at the periphery of binding interfaces (within 6.5 to 7 Å of σ3) would have little effect on the binding interaction. A panel of 30 NgR1 point mutations was engineered and screened for cell-surface expression, and the 23 mutants that were detected at the cell-surface comparable to wild-type (WT) NgR1 were included for further analyses (Fig. 6*E*). As predicted, the majority of well-expressed close-proximity mutants allowed little-to-no virus binding (Fig. 6*F*) and infectivity (Fig. 6*G*), whereas the majority of mutants with alterations at the periphery of the interaction interface conferred efficient virus binding and infectivity. Interestingly, several mutants from both classes appear to promote more efficient infection than WT NgR1 (Fig. 6*G*), which in some cases may be due to increased cell-surface expression (Fig. 6*E*) or perhaps a higher affinity interaction is established with a positively charged arginine interacting with the relatively negatively charged surface of σ3 (*SI Appendix*, Fig. S7). Receptor residues that are required for virus binding and infection (labelled in purple, Fig. 6 *C* and *D*) were mapped onto the structure alongside residues not required for virus–receptor interactions (labeled in black, Fig. 6 *C* and *D*). This analysis confirmed the molecular footprints of NgR1 binding to the $\sigma3_A$ and $\sigma3_B$ surfaces, as these defined clusters of critical residues align well with the predicted binding patches (surfaces shaded in blue, Fig. 6 *C* and *D*). Collectively, these data validate the observed cryo-EM reconstruction, highlight residues essential for interaction between receptor and virus, and provide clues about how NgR1 serves as a scaffold to bind multiple proteins simultaneously in the CNS.

Discussion

All viruses must specifically engage host cell-surface molecules to achieve reliable membrane apposition and cell entry. In this study, we evaluated biophysical parameters of reovirus binding to NgR1 and functional outcomes of this interaction. Collectively, our results reveal high-affinity interactions between reovirus virions and the human neuronal receptor NgR1 as well as an unusual binding mode for virus–receptor interactions in which NgR1 nestles between two adjacent capsid proteins. These studies expand our understanding of the reovirus capsid components used to bind cells and highlight the complex and multimodal strategy in which reovirus engages several receptors using different capsid components to promote efficient infection.

In addition to the function of NgR1 binding identified here, reovirus σ3 has several other important activities during viral replication. As a component of incoming virion particles, σ3 functions as a protector protein for the underlying μ1 membrane-penetration protein. The σ3 protein must first be cleaved and removed from virions by intestinal or endosomal proteases to expose the μ1 protein and allow subsequent entry steps (1). Opposite ends of σ3 simultaneously coordinate binding to NgR1 and μ1, and how NgR1 alters σ3 conformation, cleavage, or disassembly and other early entry steps remains to be determined. As NgR1 is GPI-anchored and has no cytoplasmic domain, intracellular signaling following NgR1 ligand binding is mediated by NgR1 coreceptors on neurons. Several coreceptors have been described (58–61), but it is not known whether these proteins function in reovirus binding or infection. We identified one NgR1 mutant (NgR1-Q211R) that allows moderate reovirus binding to cells but does not permit infection, suggesting a role for NgR1 in post-binding functions.

In the CNS, NgR1 binds a large and structurally diverse group of coreceptors and myelin-associated inhibitory ligands to control neuronal shaping. While there is a rich understanding of functional outcomes for these interactions, the structural basis underlying how diverse ligands coordinate or compete for NgR1 is lacking. Although structural data are available for many individual components (62–64), to our knowledge, only one structure has been determined of NgR1 in complex with a nonantibody ligand (65). Here, we report the structure of NgR1 bound to a viral pathogen. Reovirus engages N-terminal, LR surfaces of NgR1 at two distinct sites (Fig. 6*B* and Movie S1). A small patch on the convex face of NgR1 (Fig. 6 *B* and *C*) coordinates with a broad patch of residues on the concave face of NgR1 (Fig. 6 *B* and *D*) to imbed NgR1 between two molecules of σ3 (Figs. 5*F* and 6 *A* and *B*). Mutagenesis studies confirm a requirement of residues on

Downloaded from https://www.pnas.org by UNIVERSITE CATHOLIQUE DE LOUVAIN (UCL) SERVICE CENTRAL DES BIBLIOTHEQUES on January 16, 2024 from IP address 130.104.43.178.

Downloaded from https://www.pnas.org by UNIVERSITE CATHOLIQUE DE LOUVAIN (UCL) SERVICE CENTRAL DES BIBLIOTHEQUES on January 16, 2024 from IP address 130.104.43.178.

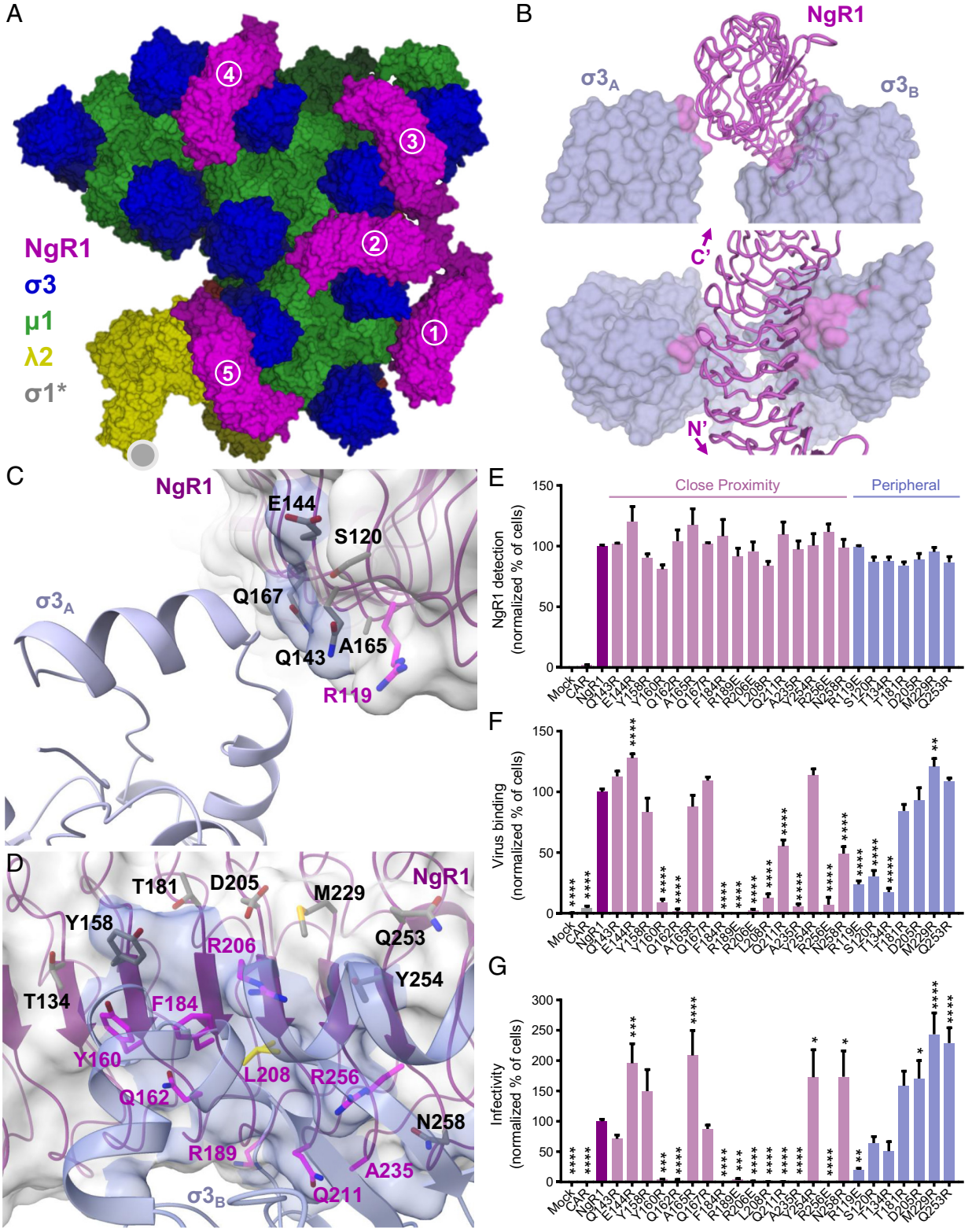

Fig. 6. NgR1 residues required for interaction with reovirus validated by structure-guided mutagenesis. (*A*) Surface representation of the modeled asymmetric unit of a reovirus virion in complex with NgR1 (extracted from Fig. 5 molecular docking). NgR1 is colored in magenta, σ3 in blue, μ1 in green, λ1 in yellow, and σ2 and λ1 in red. The approximate location at which σ1 imbeds into λ2 is depicted by a gray circle. (*B*) Interactions of NgR1 with two σ3 monomers (labeled $\sigma3_A$ and $\sigma3_B$) from different heterohexamers are depicted in a side view (*Top*) and top view (*Bottom*). NgR1 is shown as a ribbon tracing (magenta) and σ3 as a surface representation (blue). The σ3 surface < 5 Å from the NgR1 protein model is colored in magenta. (*C* and *D*) Enlarged views of the $\sigma3_A$ (*C*) and $\sigma3_B$ (*D*) interaction sites. NgR1 amino acids in proximity to σ3 are shown in stick representation. NgR1 surfaces less than 5 Å from σ3 are colored in light blue. Residue color and label color reflect mutant phenotype: purple = reduced infectivity and gray/black = normal or increased infectivity. Residue L208 is highlighted in yellow. (*E–G*) CHO cells were mock-transfected or transfected with the cDNAs shown. NgR1 mutants are labeled by the residue changed and grouped by close proximity (less than 5 Å from σ3; light purple) or peripheral (6.5 to 7 Å from σ3; light blue). (*E*) NgR1 expression, (*F*) reovirus binding, and (*G*) reovirus infectivity were determined. Shown are mean values of five or more independent experiments. Error bars indicate SEM. Values that differ significantly from NgR1 by one-way ANOVA and Dunnett's test are indicated (*P < 0.05; **P < 0.01; ***P < 0.001; ****P < 0.001).

both surfaces for reovirus binding and infectivity (Fig. 6 *E* and *F*). Interestingly, genetic (52, 66) and structural (65) studies indicate that most binding partners of NgR1 similarly require N-terminal LR sequences (a.a. 26 to 310) for binding, suggesting that virus-targeted sites on NgR1 overlap with those engaged by ligands on neurons, oligodendrocytes, and other cells in the CNS.

A key remaining question is why do reovirus, myelin-associated inhibitory ligands, and even some NgR1 coreceptors target (66) and even compete (31) for these central LR surfaces? One explanation is the high conservation of sequences on the concave NgR1 LR surface (46, 47). As NgR1 serves important functions in both the developing and mature CNS, maintenance of ligand interactions is likely to foster sequence conservation at these interfaces. In line with this idea, single-nucleotide polymorphisms of NgR1 in human populations have been associated with schizophrenia and other neurologic disorders (67–69). Indeed, many viruses, including reovirus (21), benefit from engaging protein surfaces that are required for interactions with host proteins, and thus are strictly conserved. Unlike human NgR1 studied here, murine NgR1 does not serve as an efficient reovirus receptor (70). While the broad NgR1–$\sigma3_B$ interface is highly conserved, four NgR1 polymorphisms exist at or near the smaller $\sigma3_A$ interface that may contribute to this difference in receptor use (*SI Appendix*, Fig. S8), further highlighting the importance of bimodal engagement of σ3 by conserved sequences in NgR1.

An alternative hypothesis for redundant NgR1 sequence targeting is that the residues engaged by reovirus and other NgR1 ligands are those most readily available. While most viruses appear to bind the most membrane-distal surface of a receptor (71–78), there are few examples of virus binding to lateral receptor surfaces (79, 80). The precise orientation of NgR1 on the cell surface is not known. However, we hypothesize that the concave NgR1 surface faces toward ligands on neighboring cells. This hypothesis is consistent with the identification of a hydrophobic pocket at the base of the convex surface of NgR1 (46), which may interact with the unresolved NgR1 GPI-CT structure to distance the ligand-binding face from the membrane and allow display of the expansive concave surface for efficient ligand interactions. This NgR1 positioning could explain the unusual *en face* arrangement of NgR1 on reovirus virions that we observe (Figs. 5*F* and 6*A*). Additionally, clustering of NgR1 C termini at the center of $\sigma3_3\mu1_3$ heterohexamers (Fig. 5*F*) suggests that NgR1 interacts with itself in a complex to engage reovirus, which could promote higher avidity binding. Consistent with this model, there is evidence that NgR1 forms homophilic interactions (32, 81) and that NgR1 is not broadly distributed in the membrane but instead clusters in lipid-rich microdomains that also are enriched in NgR1 coreceptors and signaling molecules (82, 83). Thus, NgR1–NgR1 interactions and lipid raft localization may influence reovirus binding and internalization. Additional studies of the GPI-CT structure and its involvement in NgR1 conformation and localization will be required to answer these questions.

Reovirus interacts with several cellular receptors using distinct capsid components. The fiber-like σ1 viral attachment protein engages sialylated glycans and JAM-A (12, 13, 20, 21), while the pentameric λ2 protein engages β1 integrins (25). We found that NgR1 serves as a receptor for reovirus σ3, which expands our understanding of reovirus interactions with host cells. Interestingly, our studies also reveal yet another parallel of reovirus structure and function with adenoviruses (84, 85), which engage CAR and sialylated glycans, integrins, and CD46 receptors using fiber (76), penton (86), and hexon (80) structural proteins, respectively. These shared similarities demonstrate how some viruses have evolved the use of all surface-exposed capsid components as receptor-binding proteins and highlight the critical importance of receptor engagement during pathogen invasion.

While human NgR1 serves as an efficient receptor for reovirus in cultured cells and appears to promote reovirus infection of human neurons (*SI Appendix*, Fig. S9), reovirus is rarely associated with neurologic disease in humans. In contrast, newborn mice are exquisitely sensitive to reovirus-induced disease, but murine NgR1 does not promote efficient reovirus binding or infectivity in cultured cells (70). We find this dichotomy intriguing. The extremely broad host range of reovirus in nature raises the possibility that NgR1 homologs from some species function as reovirus receptors and mediate reovirus disease, which is supported by a study suggesting that NgR1 is required for reovirus infection of neurons isolated from the Chinese tree shrew (87). In other species, additional receptors may function analogously to NgR1 and facilitate neuronal infection and consequent neuropathogenesis (88). A robust analysis of viral and host sequences required for reovirus–NgR1 interactions and functionality is warranted to understand how NgR1 influences both target cell selection and disease in animal models and humans.

Reovirus tropism for neurons and capacity for neurovirulence in mice are exquisitely dictated by sequences in T3 σ1 (11). Consistent with previous findings (26), we observe no preference for engagement of NgR1 by T3 sequences (Fig. 4 *E* and *F*). In fact, T1L σ3 may bind NgR1 with slightly higher probability than does T3D σ3 (*SI Appendix*, Fig. S1*A*), a property that may be conferred by σ3 polymorphisms at or near NgR1-binding sites in σ3 (*SI Appendix*, Fig. S10). These data and the absence of efficient engagement of murine NgR1 by reovirus (70) provide additional evidence that other receptors are bound by reovirus in vivo to cause encephalitis in mice. However, not all neurotropic orthoreoviruses target neurons in a σ1-dependent fashion. Baboon reovirus (BRV), which causes encephalitis in baboons (89, 90), lacks a σ1-like attachment protein but otherwise resembles reovirus structurally (91). BRV and other relatives of the strains tested here should be evaluated for binding to NgR1.

As NgR1 expression is a marker for poor prognosis in head and neck cancers in humans (92), and NgR1 expression influences susceptibility of human cancer cells to reovirus infection (26) and may influence reovirus infection of human neurons (*SI Appendix*, Fig. S9), this work reveals avenues to design improved reovirus oncolytics, which are based on the T3D strain used here (93, 94), or vector-based therapies. Moreover, studies presented in this report may inform an understanding of how NgR1 engages structurally diverse ligands and, furthermore, how these interactions influence functions of NgR1 in shaping CNS physiology.

Materials and Methods

Viruses. Reovirus strains T1L and T3D are prototype T1 and T3 viruses that were originally isolated from children (95). Strains T3SA+ and T3SA− are engineered recombinant strains (11) that express nine gene segments of T1L (including the σ3-encoding S4 gene) and the S1 gene of either T3 clone-44-MA or T3 clone-44 (96), respectively. T3SA+ and T3SA− virions differ by a single amino acid polymorphism (σ1-P204L) that abrogates the sialic acid–binding capacity of the σ1 protein (96). All viruses were recovered using plasmid-based reverse genetics (97, 98). Virus was purified from infected L929 cells by cesium chloride gradient centrifugation (99). Cryo-EM analysis indicates that greater than 98% of purified particles are virions. Viral titers were determined by particle number [estimated by spectral absorbance at 260 nm (1 OD^{260} = 2.1 × 10^{12} particles/mL)] or plaque assay in the absence of exogenous proteases and presence of FBS (99).

Force-Distance-Based AFM Using Model Surface. Force-distance curve-based AFM experiments using model surfaces were conducted in phosphate-buffered saline (PBS) at room temperature using virus-functionalized MSCT-D probes

Downloaded from https://www.pnas.org by UNIVERSITE CATHOLIQUE DE LOUVAIN (UCL) SERVICE CENTRAL DES BIBLIOTHEQUES on January 16, 2024 from IP address 130.104.43.178.

[spring constants were calculated using thermal tune (100), with values ranging from 0.030 to 0.047 N/m]. Force-Robot300 (Bruker, Germany) and NanoScope Multimode 8 (Bruker, NanoScope software v9.1) atomic force microscopes were operated in the force-volume (contact) mode. Gold-coated surfaces grafted with NgR1 were mounted on a piezoelectric scanner using a magnetic carrier. All experiments were conducted in PBS, and areas of 5 × 5 μm were scanned, with 32 × 32-pixel resolution (corresponding to 1,024 force-distance curves) and a ramp size set to 500 nm. The approach velocity was kept constant at 1 μm/s, and the maximum force was set to 500 pN.

DFS experiments to measure multiple loading rates were conducted by varying retraction speeds, set to 0.1, 0.2, 1.0, 5.0, 10, and 20 μm/s with no surface delay. Kinetic on-rate (k_{on}) measurements were conducted by recording the binding probability for hold times of 0, 50, 100, 150, 250, 500, and 1,000 ms, allowing the tip to stay in contact with the surface for different intervals.

As an independent negative control, surface blocking was conducted by incubating surfaces with NgR1-specific antibody (R&D Systems; 100 μg/mL). Measurements were obtained at a retraction velocity of 1 μm/s, before and after antibody addition. The same sample area was probed several times, using the same tip, with no surface delay.

Force-Distance-Based AFM and Fluorescence Microscopy Using Living Cells. Force-distance, curve-based AFM experiments using living cells were conducted by acquiring correlative images with an inverted epifluorescence microscope (Zeiss Observer Z.1) coupled to an atomic force microscope (Bioscope Resolve, Bruker) operated in the PeakForce Quantitative Nanomechanical Mapping mode (NanoScope software, v9.2). The atomic force microscope was equipped with a 150-μm piezoelectric scanner. A 40× oil objective (NA = 0.95) was used for imaging. Cells were maintained in growth medium at 37 °C. A gas mixture supplemented with 5% CO_2 and 95% relative humidity was infused at 0.1 L/min into the chamber. PFQNM-LC cantilevers (Bruker) were oscillated at 0.25 kHz with an amplitude of 750 nm. The sensitivity of each cantilever was calculated using the thermal noise method. Images were taken at 256 × 256 pixels, probing an area of 25 to 30 μm, with imaging forces of 500 pN and a scan frequency of 0.125 Hz.

As an independent negative control, NgR1-specific antibody (R&D Systems; 50 μg/mL) was added to medium. All other experimental parameters were maintained, and data were collected before and after antibody addition.

Receptor cDNA Transfection and Infection of CHO Cells. The day before transfection, 10^5 CHO cells/well were seeded into 24-well tissue-culture plates. Cells were transfected with cDNA using FuGene 6 (Promega, E2691) following the manufacturer's instructions using a ratio of 0.5 μg of plasmid:1.5 μL FuGene 6 (Promega, E2691) in Opti-MEM (Gibco). Mock-transfected cells were treated with Opti-MEM and FuGene 6. Cells were incubated at 37 °C for 48 h posttransfection before infection or flow cytometric analyses.

Transfected CHO cells were inoculated with T3SA− diluted in $PBS^{-/-}$ at an MOI of 10 PFU/cell and incubated at 37 °C for 1 h. The inoculum was removed, and cells were incubated in completed Ham's F12 medium. At 24 hpi, cells were washed with $PBS^{-/-}$ and fixed with cold methanol at −20 °C for at least 30 min. Fixed cells were washed and incubated with reovirus polyclonal antiserum diluted in 0.5% Triton X-100 in PBS, followed by incubation with Alexa Fluor 488-labeled secondary IgG. Cells were counterstained with DAPI and imaged at 10X using a Lionheart FX automated imaging system (BioTek). Infected cells fluorescent focus unit (FFU) were enumerated per field of view for at least four fields per well in duplicate or triplicate wells.

Flow Cytometry Assessment of Reovirus Binding or Receptor Expression. Monolayers of mock- or cDNA-transfected CHO cells were washed with PBS, detached using CellStripper Dissociation Reagent (Corning), and quenched with an equal volume of $PBS^{-/-}$ supplemented to contain 2% FBS (FACS buffer). All further incubations, washes, and pelleting were conducted in racked titer tubes (Bio-Rad; 2239391) on ice or at 4 °C. Washes and virus incubations were conducted in $PBS^{-/-}$, and antibody incubations were conducted in FACS buffer. Cells were pelleted at 500 × *g* at 4 °C for 3 min, washed, and resuspended with T3SA− (10^5 particles/cell) on ice for 1 h. Cells were pelleted, washed 3× with $PBS^{-/-}$ to remove unbound virus, and incubated with reovirus-, NgR1-, or mixed NgR1/NgR2-specific antibodies at 4 °C for 1 h. Cells were washed 3×, stained with Alexa-labeled secondary antibody at 4 °C for 1 h, and washed again 3×. Cells were fixed in $PBS^{-/-}$ supplemented to contain 1% paraformaldehyde and analyzed by flow cytometry. Results were quantified using FlowJo software. If technical repeats differed from one another by more than 50% percent, an experimental error was assumed, and the data were excluded from analyses.

Expression of ^{35}S-Labeled σ3. In vitro transcription and translation reactions were conducted using the TNT-coupled rabbit reticulocyte lysate system (Promega, L4610) according to the manufacturer's instructions. Reactions were supplemented with RNasin Plus RNase Inhibitor (N2611) and [^{35}S]-methionine (PerkinElmer, NEG709A500UC). Plasmids encoding T1L or T3D σ3 were added, and reactions were incubated at 30 °C for 1 to 1.5 h. Translation reactions were terminated with threefold excess of stop buffer (20 mM HEPES-KOH [pH 7.4], 100 mM potassium acetate, 5 mM magnesium acetate, 5 mM EDTA, 2 mM unlabeled methionine) supplemented prior to use with a final concentration of 1 mM dithiothreitol and 2 mM puromycin.

Immunoprecipitations of Purified Proteins. Buffer (beads-alone control) or 5 μg of antibody (10C1 or 8H6) or Fc-conjugated protein (CAR-Fc, JAM-A-Fc, NgR1(1-447)-Fc, or NgR1(1-310)-Fc) was added to either stop-buffer-diluted lysates expressing T1L or T3D ^{35}S-σ3 (28 μL) or purified heterohexamer (0.8 μg) in a total volume of 50 μL and incubated at 4 °C for 1 h with rotation. Samples were incubated with protein G Dynabeads (50 μL) at 4 °C for 1 h with rotation. Beads were washed at least four times with Tris-buffered saline (20 mM Tris-HCl pH 7.5, 150 mM NaCl) containing 0.05% Tween-20 (σ3) or PBS (heteroxamer) and transferred to new tubes prior to boiling at 95 °C for 5 min. Released proteins were subjected to SDS-PAGE.

Detailed information about cell growth conditions, antibodies, recombinant DNA, preparation of tips and model surfaces for AFM, gel and membrane approaches, protein purification, cryo-EM, and data analyses can be found in *SI Appendix*.

Data, Materials, and Software Availability. The cryo-EM 3D reconstruction data from this publication have been deposited with the Electron Microscopy Data Bank (https://www.ebi.ac.uk/emdb/) and assigned the following accession codes: reovirus + NgR1 (EMD-13149) (101) and reovirus alone (EMD-13150) (102). All other data are included in the manuscript or *SI Appendix*.

ACKNOWLEDGMENTS. We thank the Vanderbilt Antibody and Protein Resource for production and purification of some of the Fc-tagged proteins. We thank Stephen C. Harrison and Tobias Herrmann for providing purified heterohexamer protein. We thank Z. Hong Zhou for providing the atomic coordinates of PDB entries *7ell* and *7elh* prior to official release. This work was supported by the U.S. Public Health Service awards T32 AI007281 (D.M.S.), R01 AI038296 (D.M.S. and T.S.D.), R01 AI118887 (D.M.S., T.S., and T.S.D.), R01 AI174526 (D.M.S., B.V.V.P., and T.S.D.),R01 GM143380 (Z.W.),and R01 HL162842 (Z.W.). Additional support was provided by The Robert A. Welch Foundation (grant no. Q-2173-20230405) (Z.W.) and by University of Pittsburgh Medical Center Children's Hospital of Pittsburgh (P.A.) and the Heinz Endowments (T.S.D.). Support (M.K., R.d.S.N., and D.A.) also was contributed by the Universiteì catholique de Louvain, the Fonds National de la Recherche Scientifique (F.R.S.-FNRS), the European Research Council by the European Union's Horizon 2020 research and innovation program (grant no. 758224), and the FNRS-Welbio (grant no. CR-2019S-01). M.K. (Postdoctoral Researcher) and D.A. (Research Associate) are members of the FNRS. The Baylor College of Medicine Cryo-Electron Microscopy and Tomography Core, an Advanced Technology Core, was supported by the Cancer Prevention and Research Institute of Texas (grant no. RP190602). The funders had no role in study design, data collection and analysis, decision to publish, or preparation of the manuscript.

Author affiliations: [a]Department of Pediatrics, University of Pittsburgh School of Medicine, Pittsburgh, PA 15224; [b]Institute of Infection, Inflammation, and Immunity, University of Pittsburgh Medical Center Children's Hospital of Pittsburgh, Pittsburgh, PA 15224; [c]Interfaculty Institute of Biochemistry, University of Tübingen, D-72076 Tübingen, Germany; [d]Louvain Institute of Biomolecular Science and Technology, Université catholique de Louvain, 1348 Louvain-la-Neuve, Belgium; [e]Verna and Marrs McLean Department of Biochemistry and Molecular Biology, Baylor College of Medicine, Houston, TX 77030; [f]Cryo-Electron Microscopy and Tomography Core, Baylor College of Medicine, Houston, TX 77030; [g]Department of Pathology, Microbiology, and Immunology, Vanderbilt University School of Medicine, Nashville, TN 37232; [h]Department of Human Genetics, University of Pittsburgh School of Public Health, Pittsburgh, PA 15261; [i]Children's Neuroscience Institute, University of Pittsburgh Medical Center Children's Hospital of Pittsburgh, Pittsburgh, PA 15224; [j]Walloon Excellence in Life Sciences and Biotechnology, 1300 Wavre, Belgium; [k]Department of Molecular and Cellular Biology, Baylor College of Medicine, Houston, TX 77030; [l]Department of Molecular Virology and Microbiology, Baylor College of Medicine, Houston, TX 77030; and [m]Department of Microbiology and Molecular Genetics, University of Pittsburgh School of Medicine, Pittsburgh, PA 15219

Downloaded from https://www.pnas.org by UNIVERSITE CATHOLIQUE DE LOUVAIN (UCL) SERVICE CENTRAL DES BIBLIOTHEQUES on January 16, 2024 from IP address 130.104.43.178.

1. A. N. Roth *et al.*, Ins and outs of reovirus: Vesicular trafficking in viral entry and egress. *Trends Microbiol.* **29**, 363–375 (2021).
2. G. Margolis, L. Kilham, Hydrocephalus in hamsters, ferrets, rats, and mice following inoculations with reovirus type I. II. Pathologic studies. *Lab Invest.* **21**, 189–198 (1969).
3. C. S. Raine, B. N. Fields, Reovirus type 3 encephalitis-a virologic and ultrastructural study. *J. Neuropathol. Exp. Neurol.* **32**, 19–33 (1973).
4. A. G. Wu *et al.*, Age-dependent susceptibility to reovirus encephalitis in mice is influenced by maturation of the type-I interferon response. *Pediatr. Res.* **83**, 1057–1066 (2018).
5. A. M. Lerner, J. D. Cherry, J. O. Klein, M. Finland, Infections with reoviruses. *N. Engl. J. Med.* **267**, 947–952 (1962).
6. S. C. Richardson, R. F. Bishop, A. L. Smith, Reovirus serotype 3 infection in infants with extrahepatic biliary atresia or neonatal hepatitis. *J. Gastroenterol. Hepatol.* **9**, 264–268 (1994).
7. B. Selb, B. Weber, A study of human reovirus IgG and IgA antibodies by ELISA and western blot. *J. Virological Methods* **47**, 15–25 (1994).
8. J. H. Tai *et al.*, Prevalence of reovirus-specific antibodies in young children in Nashville, Tennessee. *J. Infect. Dis.* **191**, 1221–1224 (2005).
9. C. Masters, M. Alpers, B. Kakulas, Pathogenesis of reovirus type 1 hydrocephalus in mice. Significance of aqueductal changes. *Arch. Neurol.* **34**, 18–28 (1977).
10. H. L. Weiner, D. Drayna, D. R. Averill Jr., B. N. Fields, Molecular basis of reovirus virulence: Role of the S1 gene. *Proc. Natl. Acad. Sci. U.S.A.* **74**, 5744–5748 (1977).
11. D. M. Sutherland, P. Aravamudhan, M. H. Dietrich, T. Stehle, T. S. Dermody, Reovirus neurotropism and virulence are dictated by sequences in the head domain of the viral attachment protein. *J. Virol.* **92**, e00974–00918 (2018).
12. D. M. Reiter *et al.*, Crystal structure of reovirus attachment protein s1 in complex with sialylated oligosaccharides. *PLoS Pathog.* **7**, e1002166 (2011).
13. K. Reiss *et al.*, The GM2 glycan serves as a functional co-receptor for serotype 1 reovirus. *PLoS Pathog.* **8**, e1003078 (2012).
14. E. S. Barton, J. L. Connolly, J. C. Forrest, J. D. Chappell, T. S. Dermody, Utilization of sialic acid as a coreceptor enhances reovirus attachment by multistep adhesion strengthening. *J. Biol. Chem.* **276**, 2200–2211 (2001).
15. M. Koehler *et al.*, Glycan-mediated enhancement of reovirus receptor binding. *Nat. Commun.* **10**, 4460 (2019).
16. J. L. Connolly, E. S. Barton, T. S. Dermody, Reovirus binding to cell surface sialic acid potentiates virus-induced apoptosis. *J. Virol.* **75**, 4029–4039 (2001).
17. J. Stencel-Baerenwald *et al.*, Glycan engagement dictates hydrocephalus induction by serotype 1 reovirus. *mBio* **6**, e02356–02314 (2015).
18. J. M. Frierson *et al.*, Utilization of sialylated glycans as coreceptors enhances the neurovirulence of serotype 3 reovirus. *J. Virol.* **86**, 13164–13173 (2012).
19. E. S. Barton *et al.*, Utilization of sialic acid as a coreceptor is required for reovirus-induced biliary disease. *J. Clin. Invest.* **111**, 1823–1833 (2003).
20. E. Stettner, M. H. Dietrich, K. Reiss, T. S. Dermody, T. Stehle, Structure of serotype 1 reovirus attachment protein s1 in complex with junctional adhesion molecule A reveals a conserved serotype-independent binding epitope. *J. Virol.* **89**, 6136–6140 (2015).
21. E. Kirchner, K. M. Guglielmi, H. M. Strauss, T. S. Dermody, T. Stehle, Structure of reovirus s1 in complex with its receptor junctional adhesion molecule-A. *PLoS Pathog.* **4**, e1000235 (2008).
22. C. M. Lai *et al.*, Endothelial JAM-A promotes reovirus viremia and bloodstream dissemination. *J. Infect. Dis.* **211**, 383–393 (2015).
23. A. A. R. Antar *et al.*, Junctional adhesion molecule-A is required for hematogenous dissemination of reovirus. *Cell Host Microbe.* **5**, 59–71 (2009).
24. M. S. Maginnis *et al.*, b1 integrin mediates internalization of mammalian reovirus. *J. Virol.* **80**, 2760–2770 (2006).
25. M. Koehler *et al.*, Reovirus directly engages integrin to recruit clathrin for entry into host cells. *Nat. Commun.* **12**, 2149 (2021).
26. J. L. Konopka-Anstadt *et al.*, The Nogo receptor NgR1 mediates infection by mammalian reovirus. *Cell Host Microbe.* **15**, 681–691 (2014).
27. X. Wang *et al.*, Localization of Nogo-A and Nogo-66 receptor proteins at sites of axon-myelin and synaptic contact. *J. Neurosci.* **22**, 5505–5515 (2002).
28. S. M. Oberhaus, R. L. Smith, G. H. Clayton, T. S. Dermody, K. L. Tyler, Reovirus infection and tissue injury in the mouse central nervous system are associated with apoptosis. *J. Virol.* **71**, 2100–2106 (1997).
29. G. Smedfors, L. Olson, T. E. Karlsson, A nogo-like signaling perspective from birth to adulthood and in old age: Brain expression patterns of ligands, receptors and modulators. *Front. Mol. Neurosci.* **11**, 42 (2018).
30. A. E. Fournier, T. GrandPre, S. M. Strittmatter, Identification of a receptor mediating Nogo-66 inhibition of axonal regeneration. *Nature* **409**, 341–346 (2001).
31. M. Domeniconi *et al.*, Myelin-associated glycoprotein interacts with the Nogo66 receptor to inhibit neurite outgrowth. *Neuron* **35**, 283–290 (2002).
32. B. P. Liu, A. Fournier, T. GrandPre, S. M. Strittmatter, Myelin-associated glycoprotein as a functional ligand for the Nogo-66 receptor. *Science* **297**, 1190–1193 (2002).
33. K. C. Wang *et al.*, Oligodendrocyte-myelin glycoprotein is a Nogo receptor ligand that inhibits neurite outgrowth. *Nature* **417**, 941–944 (2002).
34. A. Hanell *et al.*, Genetic deletion and pharmacological inhibition of Nogo-66 receptor impairs cognitive outcome after traumatic brain injury in mice. *J. Neurotrauma* **27**, 1297–1309 (2010).
35. S. Li *et al.*, Blockade of Nogo-66, myelin-associated glycoprotein, and oligodendrocyte myelin glycoprotein by soluble Nogo-66 receptor promotes axonal sprouting and recovery after spinal injury. *J. Neurosci.* **24**, 10511–10520 (2004).
36. X. Wang *et al.*, Recovery from chronic spinal cord contusion after Nogo receptor intervention. *Annals Neurol.* **70**, 805–821 (2011).
37. J. K. Lee, B. Zheng, Role of myelin-associated inhibitors in axonal repair after spinal cord injury. *Exp. Neurol.* **235**, 33–42 (2012).
38. L. A. Breun *et al.*, Mammalian reovirus L2 gene and l2 core spike protein sequences and whole-genome comparisons of reoviruses type 1 Lang, type 2 Jones, and type 3 Dearing. *Virology* **287**, 333–348 (2001).
39. D. Alsteens *et al.*, Nanomechanical mapping of first binding steps of a virus to animal cells. *Nat. Nanotechnol.* **12**, 177–183 (2017).
40. E. Evans, K. Ritchie, Dynamic strength of molecular adhesion bonds. *Biophys. J.* **72**, 1541–1555 (1997).
41. G. I. Bell, Models for the specific adhesion of cells to cells. *Science* **200**, 618–627 (1978).
42. E. Evans, P. Williams, *Physics of bio-molecules and cells, Ecole d'Ete de Physique Theorique book series* (Springer, 2001), **vol. 75**.
43. C. Rankl *et al.*, Multiple receptors involved in human rhinovirus attachment to live cells. *Proc. Natl. Acad. Sci. U.S.A.* **105**, 17778–17783 (2008).
44. E. S. Barton *et al.*, Junction adhesion molecule is a receptor for reovirus. *Cell* **104**, 441–451 (2001).
45. S. L. Deutscher, N. Nuwayhid, P. Stanley, E. I. Briles, C. B. Hirschberg, Translocation across Golgi vesicle membranes: A CHO glycosylation mutant deficient in CMP-sialic acid transport. *Cell* **39**, 295–299 (1984).
46. X. L. He *et al.*, Structure of the Nogo receptor ectodomain: A recognition module implicated in myelin inhibition. *Neuron* **38**, 177–185 (2003).
47. W. A. Barton *et al.*, Structure and axon outgrowth inhibitor binding of the Nogo-66 receptor and related proteins. *Embo. J.* **22**, 3291–3302 (2003).
48. I. Botos, D. M. Segal, D. R. Davies, The structural biology of Toll-like receptors. *Structure* **19**, 447–459 (2011).
49. V. Motta, F. Soares, T. Sun, D. J. Philpott, NOD-like receptors: Versatile cytosolic sentinels. *Physiol. Rev.* **95**, 149–178 (2015).
50. B. W. Han, B. R. Herrin, M. D. Cooper, I. A. Wilson, Antigen recognition by variable lymphocyte receptors. *Science* **321**, 1834–1837 (2008).
51. T. L. Dickendesher *et al.*, NgR1 and NgR3 are receptors for chondroitin sulfate proteoglycans. *Nat. Neurosci.* **15**, 703–712 (2012).
52. K. Venkatesh *et al.*, The Nogo-66 receptor homolog NgR2 is a sialic acid-dependent receptor selective for myelin-associated glycoprotein. *J. Neurosci.* **25**, 808–822 (2005).
53. J. Lauren, M. S. Airaksinen, M. Saarma, T. Timmusk, Two novel mammalian Nogo receptor homologs differentially expressed in the central and peripheral nervous systems. *Mol. Cell. Neurosci.* **24**, 581–594 (2003).
54. M. Semavina *et al.*, Crystal structure of the nogo-receptor-2. *Protein. Sci.* **20**, 684–689 (2011).
55. A. M. Olland, J. Jané-Valbuena, L. A. Schiff, M. L. Nibert, S. C. Harrison, Structure of the reovirus outer capsid and dsRNA-binding protein s3 at 1.8 Å resolution. *Embo J.* **20**, 979–989 (2001).
56. X. Zhang, S. B. Walker, P. R. Chipman, M. L. Nibert, T. S. Baker, Reovirus polymerase l3 localized by cryo-electron microscopy of virions at a resolution of 7.6 A. *Nat. Struct. Biol.* **10**, 1011–1018 (2003).
57. M. Pan *et al.*, Asymmetric reconstruction of mammalian reovirus reveals interactions among RNA, transcriptional factor μ2 and capsid proteins. *Nat Commun* **12**, 4176 (2021).
58. Z. Ahmed, M. R. Douglas, G. John, M. Berry, A. Logan, AMIGO3 is an NgR1/p75 co-receptor signalling axon growth inhibition in the acute phase of adult central nervous system injury. *PloS one* **8**, e61878 (2013).
59. S. Mi *et al.*, LINGO-1 is a component of the Nogo-66 receptor/p75 signaling complex. *Nat. Neurosci.* **7**, 221–228 (2004).
60. K. C. Wang, J. A. Kim, R. Sivasankaran, R. Segal, Z. He, P75 interacts with the Nogo receptor as a co-receptor for Nogo, MAG and OMgp. *Nature* **420**, 74–78 (2002).
61. Z. Shao *et al.*, TAJ/TROY, an orphan TNF receptor family member, binds Nogo-66 receptor 1 and regulates axonal regeneration. *Neuron* **45**, 353–359 (2005).
62. M. Li, J. Liu, J. Song, Nogo goes in the pure water: Solution structure of Nogo-60 and design of the structured and buffer-soluble Nogo-54 for enhancing CNS regeneration. *Protein Sci.* **15**, 1835–1841 (2006).
63. L. Mosyak *et al.*, The structure of the Lingo-1 ectodomain, a module implicated in central nervous system repair inhibition. *J. Biol. Chem.* **281**, 36378–36390 (2006).
64. M. F. Pronker *et al.*, Structural basis of myelin-associated glycoprotein adhesion and signalling. *Nat. Commun.* **7**, 13584 (2016).
65. J. Wang *et al.*, RTN4/NoGo-receptor binding to BAI adhesion-GPCRs regulates neuronal development. *Cell* **184**, 5869–5885.e5825 (2021).
66. J. Lauren *et al.*, Characterization of myelin ligand complexes with neuronal Nogo-66 receptor family members. *J. Biol. Chem.* **282**, 5715–5725 (2007).
67. R. Hsu *et al.*, Nogo receptor 1 (RTN4R) as a candidate gene for schizophrenia: Analysis using human and mouse genetic approaches. *PloS one* **2**, e1234 (2007).
68. S. Budel *et al.*, Genetic variants of Nogo-66 receptor with possible association to schizophrenia block myelin inhibition of axon growth. *J. Neurosci.* **28**, 13161–13172 (2008).
69. L. Sinibaldi *et al.*, Mutations of the nogo-66 receptor (RTN4R) gene in schizophrenia. *Hum. Mutat.* **24**, 534–535 (2004).
70. P. Aravamudhan *et al.*, The murine neuronal receptor NgR1 is dispensable for reovirus pathogenesis. *J. Virol.* **96**, e00055–00022 (2021).
71. P. D. Kwong *et al.*, Structure of an HIV gp120 envelope glycoprotein in complex with the CD4 receptor and a neutralizing human antibody. *Nature* **393**, 648–659 (1998).
72. L. Xing, J. M. Casasnovas, R. H. Cheng, Structural analysis of human rhinovirus complexed with ICAM-1 reveals the dynamics of receptor-mediated virus uncoating. *J. Virol.* **77**, 6101–6107 (2003).
73. D. M. Belnap *et al.*, Three-dimensional structure of poliovirus receptor bound to poliovirus. *Proc. Natl. Acad. Sci. U.S.A.* **97**, 73–78 (2000).
74. P. Di Giovine *et al.*, Structure of herpes simplex virus glycoprotein D bound to the human receptor nectin-1. *PLoS Pathog* **7**, e1002277 (2011).
75. T. Hashiguchi *et al.*, Structure of the measles virus hemagglutinin bound to its cellular receptor SLAM. *Nat. Struct. Mol. Biol.* **18**, 135–141 (2011).
76. Y. He *et al.*, Interaction of coxsackievirus B3 with the full length coxsackievirus-adenovirus receptor. *Nat. Struct. Biol.* **8**, 874–878 (2001).
77. C. Xiao *et al.*, Interaction of coxsackievirus A21 with its cellular receptor, ICAM-1. *J. Virol.* **75**, 2444–2451 (2001).
78. P. Zhang *et al.*, Crystal structure of CD155 and electron microscopic studies of its complexes with polioviruses. *Proc. Natl. Acad. Sci. U.S.A.* **105**, 18284–18289 (2008).
79. R. Zhang *et al.*, Mxra8 is a receptor for multiple arthritogenic alphaviruses. *Nature* **557**, 570–574 (2018), 10.1038/s41586-018-0121-3.
80. B. D. Persson *et al.*, Human species D adenovirus hexon capsid protein mediates cell entry through a direct interaction with CD46. *Proc. Natl. Acad. Sci. U.S.A.* **118**, e2020732118 (2021).
81. A. E. Fournier, G. C. Gould, B. P. Liu, S. M. Strittmatter, Truncated soluble Nogo receptor binds Nogo-66 and blocks inhibition of axon growth by myelin. *J. Neurosci.* **22**, 8876–8883 (2002).
82. W. Yu, W. Guo, L. Feng, Segregation of Nogo66 receptors into lipid rafts in rat brain and inhibition of Nogo66 signaling by cholesterol depletion. *FEBS Lett.* **577**, 87–92 (2004).
83. M. Vinson *et al.*, Lipid rafts mediate the interaction between myelin-associated glycoprotein (MAG) on myelin and MAG-receptors on neurons. *Mol. Cell. Neurosci.* **22**, 344–352 (2003).

Downloaded from https://www.pnas.org by UNIVERSITE CATHOLIQUE DE LOUVAIN (UCL) SERVICE CENTRAL DES BIBLIOTHEQUES on January 16, 2024 from IP address 130.104.43.178.

84. T. Stehle, T. S. Dermody, Structural evidence for common functions and ancestry of the reovirus and adenovirus attachment proteins. *Rev. Med. Virol.* **13**, 123–132 (2003).
85. T. Stehle, T. S. Dermody, Structural similarities in the cellular receptors used by adenovirus and reovirus. *Viral. Immunol.* **17**, 129–143 (2004).
86. C. Y. Chiu, P. Mathias, G. R. Nemerow, P. L. Stewart, Structure of adenovirus complexed with its internalization receptor, avb5 integrin. *J. Virol.* **73**, 6759–6768 (1999).
87. C. Lu *et al.*, Molecular characterization and function of the Nogo-66 Receptor (NgR1) gene in the Chinese Tree Shrew. *J. Integr. Neurosci.* **22**, 22 (2023).
88. P. Shang *et al.*, Paired immunoglobulin-like receptor B is an entry receptor for mammalian orthoreovirus. *Nat. Commun.* **14**, 2615 (2023).
89. S. Kumar *et al.*, Reovirus-associated meningoencephalomyelitis in baboons. *Veterinary pathology* **51**, 641–650 (2014).
90. M. M. Leland, G. B. Hubbard, H. T. Sentmore 3rd, K. F. Soike, J. K. Hilliard, Outbreak of orthoreovirus-induced meningoencephalomyelitis in baboons. *Comp. Med.* **50**, 199–205 (2000).
91. X. Yan *et al.*, Virion structure of baboon reovirus, a fusogenic orthoreovirus that lacks an adhesion fiber. *J. Virol.* **85**, 7483–7495 (2011).
92. H. P. A. Consortium, The Human Protein Atlas. (https://www.proteinatlas.org/) (2017).
93. T. Bourhill, Y. Mori, D. E. Rancourt, M. Shmulevitz, R. N. Johnston, Going (reo)viral: Factors promoting successful reoviral oncolytic infection. *Viruses* **10**, 421 (2018).
94. D. Clements, E. Helson, S. A. Gujar, P. W. Lee, Reovirus in cancer therapy: An evidence-based review. *Oncol. Virother.* **3**, 69–82 (2014).
95. A. B. Sabin, Reoviruses: A new group of respiratory and enteric viruses formerly classified as ECHO type 10 is described. *Science* **130**, 1387–1389 (1959).
96. J. D. Chappell, V. L. Gunn, J. D. Wetzel, G. S. Baer, T. S. Dermody, Mutations in type 3 reovirus that determine binding to sialic acid are contained in the fibrous tail domain of viral attachment protein s1. *J. Virol.* **71**, 1834–1841 (1997).
97. T. Kobayashi *et al.*, A plasmid-based reverse genetics system for animal double-stranded RNA viruses. *Cell Host Microbe.* **1**, 147–157 (2007).
98. T. Kobayashi, L. S. Ooms, M. Ikizler, J. D. Chappell, T. S. Dermody, An improved reverse genetics system for mammalian orthoreoviruses. *Virology* **398**, 194–200 (2010).
99. A. Berard, K. M. Coombs, "Mammalian reoviruses: Propagation, quantification, and storage" in *Current Protocols in Microbiology* Chapter 15, Unit15C 11 (Current Protocols, 2009).
100. H. J. Butt, M. Jaschke, Calculation of thermal noise in atomic force microscopy. *Nanotechnology* **6** (1995).
101. M. Strebl *et al.*, Mammalian orthoreovirus T3SA- in complex with the neural *receptor* NgR1. *Electron Microscopy Data Bank*. https://www.emdataresource.org/EMD-13149. Deposited 6 March 2021.
102. M. Strebl *et al.*, Mammalian orthoreovirus T3SA-. *Electron Microscopy Data Bank*. https://www.emdataresource.org/EMD-13150. Deposited 6 March 2021.

Downloaded from https://www.pnas.org by UNIVERSITE CATHOLIQUE DE LOUVAIN (UCL) SERVICE CENTRAL DES BIBLIOTHEQUES on January 16, 2024 from IP address 130.104.43.178.